# Fitting Yeast and Mammalian Prion Aggregation Kinetic Data with the Finke−Watzky Two-Step Model of Nucleation and Autocatalytic Growth[†]

Murielle A. Watzky,[‡,§] Aimee M. Morris,[‡,§] Eric D. Ross,*[,||] and Richard G. Finke*[,‡]

*Department of Chemistry and Department of Biochemistry and Molecular Biology, Colorado State University, Fort Collins, Colorado 80523*

*Received April 23, 2008; Revised Manuscript Received July 9, 2008*

ABSTRACT: Recently, we reported 14 amyloid protein aggregation kinetic data sets that were fit using the "Ockham's razor"/minimalistic Finke−Watzky (F−W) two-step model of slow nucleation (A → B, rate constant $k_1$) and fast autocatalytic growth (A + B → 2B, rate constant $k_2$), yielding quantitative (average) rate constants for nucleation ($k_1$) and growth ($k_2$), where A is the monomeric protein and B is the polymeric protein [Morris, A. M., et al. (2008) *Biochemistry 47*, 2413−2427]. Herein, we apply the F−W model to 27 representative prion aggregation kinetic data sets obtained from the literature. Each prion data set was successfully fit with the F−W model, including three different yeast prion proteins (Sup35p, Ure2p, and Rnq1p) as well as mouse and human prions. These fits yield the first quantitative rate constants for the steps of nucleation and growth in prion aggregation. Examination of a Sup35p system shows that the same rate constants are obtained for nucleation and for growth within experimental error, regardless of which of six physical methods was used, a unique set of important control experiments in the protein aggregation literature. Also provided herein are analyses of several factors influencing the aggregation of prions such as glutamine/asparagine rich regions and the number of oligopeptide repeats in the prion domain. Where possible, verification or refutation of previous correlations to glutamine/asparagine regions, or the number of repeat sequences, in literature aggregation kinetics is given in light of the quantitative rate constants obtained herein for nucleation and growth during prion aggregation. The F−W model is then contrasted to four literature mechanisms that address the molecular picture of prion transmission and propagation. Key limitations of the F−W model are listed to prevent overinterpretation of the data being analyzed, limitations that derive ultimately from the model's simplicity. Finally, possible avenues of future research are suggested.

The mammalian prion diseases (or transmissible spongiform encephalopathies) are a subset of neurodegenerative disorders that include bovine spongiform encephalopathy (or "mad cow" disease), scrapie in sheep, chronic wasting disease in deer and elk, and the human kuru and Creutzfeldt-Jakob diseases (*1*). It is generally recognized that the infectious prion agent is composed of protein (thus the term prion for *pr*oteinaceous *i*nfectious -*on*) (*2*). However, in the case of mammalian prions it has not been irrefutably shown whether the infectious agent is composed of only protein (*3, 4*). The prion agent in mammalian diseases is usually termed $PrP^{Sc}$ (for prion protein, scrapie) and the normal form of the protein as $PrP^{C}$ (for prion protein, cellular).[1] The two forms of the protein are believed to be conformational isomers (*2*), with the $PrP^{Sc}$ form believed (i) to be aggregation-prone with a secondary structure of high $\beta$-sheet character (*5*) and (ii) to have the ability to convert $PrP^{C}$ (of predominantly α-helix secondary structure) into $PrP^{Sc}$ (*1*).

The prions found in yeast are now being widely used as models of the mammalian prion diseases, as (i) they appear to propagate in a manner similar to that of their mammalian equivalent and, importantly, (ii) unlike their mammalian equivalent, they are not contagious to humans (*6*). In the yeast species *Saccharomyces cerevisiae* (*SC*), three different prions have been identified, the names of which are derived from the characteristic (change in) phenotype that accompanies them: [URE3], [*PSI*+], and [*PIN*+] (*7, 8*). The "encoding" or "determinant" proteins whose propagating prion form is associated with these prion diseases are Ure2p, Sup35p, and Rnq1p, respectively (*12*). Hence, overexpression

[†] The Finke−Watzky mechanism grew out of long-term support from DOE Grant SE-FG02-03ER15453; without that long-term support, its discovery would not have been possible. Partial support by NSF Grant 0611588 is also gratefully acknowledged. E.D.R. acknowledges funding from a March of Dimes Basil O'Connor Award (5-FY07-104) and the American Heart Association (0735321N).

* To whom correspondence should be addressed. R.G.F.: e-mail, rfinke@lamar.colostate.edu; telephone, (970) 491-2541; fax, (970) 491-1801. E.D.R.: e-mail, eric.ross@colostate.edu; telephone, (970) 491-0688; fax, (970) 491-0494.

[‡] Department of Chemistry.

[§] These authors contributed equally to this work.

[||] Department of Biochemistry and Molecular Biology.

[1] Abbreviations: ANS, ANS fluorescence; *CA*, *Candida albicans*; CHY, chymotrypsin resistance; CR, congo red; F−W, Finke−Watzky; LS, light scattering; MDC, monomer-directed conversion; NCC, nucleated conformational conversion; NP, nucleated polymerization; PrD, prion domain; $PrP^{C}$, prion protein, cellular; $PrP^{Sc}$, prion protein, scrapie; *SC*, *Saccharomyces cerevisiae*; SDS−PAGE, sodium dodecyl sulfate−polyacrylamide gel electrophoresis; Sed, sedimentation; TA, templated assembly.

10.1021/bi800726m CCC: $40.75 
Published on Web 09/12/2008

Table 1: Four Proposed Literature Mechanisms of Transmission and Propagation of the Prion Agent (*23, 30*)

| entry | ref | year | author | mechanism[a] |
|---|---|---|---|---|
| I | *29* | 1967 | J. S. Griffith | template assembly (TA) |
| II | *25*, *26* | 1991 | S. B. Prusiner | monomer-directed conversion (MDC) |
| III | *27*, *28* | 1993 | P. T. Lansbury, Jr. | nucleated polymerization (NP) |
| IV | *23* | 2000 | S. L. Lindquist | nucleated conformational conversion (NCC) |

[a] The mechanistic nomenclature comes from ref *23*.

of the protein Ure2p, Sup35p, or Rnq1p will cause de novo appearance in *SC* yeast of the prion phenotype [URE3] (*9*), [*PSI*+] (*10*), or [*PIN*+] (*11*), respectively. For the yeast prions, it has been demonstrated that the infectious prion agent is composed only of protein, as amyloid fibrils formed in vitro by purified proteins are found to be infectious when transformed into yeast (*12*−*15*).

A common feature in many neurodegenerative disorders is the presence of insoluble protein aggregate fibrils (called amyloid fibrils) in the affected area of the brain. In prion diseases, it is the prion form of the protein that aggregates to form fibrils. Fibrils are typically composed of the protein in a $\beta$-sheet secondary structure, with all $\beta$-sheets aligned perpendicular to the axis of the fibril. The final product is an insoluble fibril comprised of $\beta$-sheets; however, it is unclear if these insoluble fibrils are toxic (*16*). It it is currently believed that smaller, soluble oligomeric intermediates in the protein aggregation process are toxic to the neuronal cells, but the structure of these intermediates is still under investigation (*17, 18*). It is also not clear whether the oligomeric species that are toxic lead to the formation of ordered fibrils ("on-pathway") or instead to the formation of disordered aggregates ("off-pathway") (*19*−*22*).

The exact (molecular) mechanism of transmission and propagation of prion diseases is still controversial, but generally believed to be intimately linked to prion aggregation (*23, 24*). Overall, four different mechanisms have been proposed in the literature for how transmission and propagation of the prion disease may occur through an agent made (only) of protein (see Table 1 below). The first three mechanisms (I, II, and III) were originally developed for mammalian prion diseases (*25*−*29*) but have been widely cited in yeast prion studies. The last mechanism (IV) was proposed in a study of the yeast prion Sup35p (*23*).

These four mechanisms are often displayed as word and picture-only mechanisms that lack the numerically or analytically integrable balanced chemical equations corresponding to the proposed mechanism. This is not to say that these needed equations do not (or can not) exist, only that they are not routinely provided nor, therefore, used to fit prion aggregation kinetic data. Of course, without connecting specific balanced reactions to their corresponding differential/integrated kinetic equations, one cannot verify the postulated (word or picture-only) mechanism (*30*). In short, it remains crucial to gain a better understanding of the mechanism(s) of protein aggregation. Having a minimalistic kinetic model that can account for the available prion aggregation data is a needed, key first step toward that better understanding.

Recently, we were able to fit a broad range of amyloid protein aggregation (14 representative kinetic data sets) using the minimalistic/"Ockham's razor" Finke−Watzky (F−W) two-step model of nucleation and autocatalytic growth (*31*) (Scheme 1). With those results, we were able to obtain separate quantitative rate constants for nucleation and growth

Scheme 1: Minimalistic F−W Two-Step Model of Slow Nucleation Followed by Fast Autocatalytic Growth (*42*)[a]

$$A \xrightarrow{k_1} B$$

$$A + B \xrightarrow{k_2} 2B$$

[a] A is the monomeric form of the protein, and B is the (auto)catalytic, polymeric form of the protein.

of amyloid protein aggregation for those 14 data sets for the first time (*31*). However, due to the breadth of the protein aggregation literature, we previously focused our attention on the proteins of amyloid $\beta$, α-synuclein, and polyglutamine (*31*). We purposely, but arbitrarily, left out prion proteins in that first study (*31*).

Herein, we apply the two-step F−W model to the aggregation of prion proteins with a focus on the *SC* yeast prion proteins Ure2p, Sup35p, and Rnq1p. We report 24 representative fits of aggregation kinetics of Ure2p, Sup35p, and Rnq1p to the F−W model. We also examine three representative examples of mammalian prion aggregation kinetics using the F−W model, again affording quantitative (albeit average, vide infra) rate constants for nucleation and growth. In all cases that were examined, the F−W model is able to fit the prion aggregation kinetic data. To the best of our knowledge, this is the first nonempirical (*30*) equation that has been used to fit prion aggregation kinetic data and afford quantitative, separate (average) rate constants for both nucleation ($k_1$) and growth ($k_2$).

## MATERIALS AND METHODS

*Selection of Data Sets for Analysis.* The literature was searched, using both Scifinder Scholar and the Web of Science, for yeast prion as well as mammalian prion aggregation kinetics. For the yeast prion references, we chose representative data sets to fit from various research groups, under various conditions, and with the wild type and mutants of Ure2p, Sup35p, and Rnq1p proteins. For the mammalian prion aggregation kinetics, three representative data sets were chosen (from a small number of data sets).

*Data Analysis and Curve Fitting.* Data were extracted (digitized) from the published kinetic curves cited herein using Engauge Digitizer 2.12. All data were fit using the integrated analytical equation (eq 1) corresponding to the F−W two-step model using Origin 7.0, as detailed previously (*31*).

$$[\mathrm{B}]_t = [\mathrm{A}]_0 - \frac{\frac{k_1}{k_2} + [\mathrm{A}]_0}{1 + \frac{k_1}{k_2[\mathrm{A}]_0}\exp(k_1 + k_2[\mathrm{A}]_0)t} \qquad (1)$$

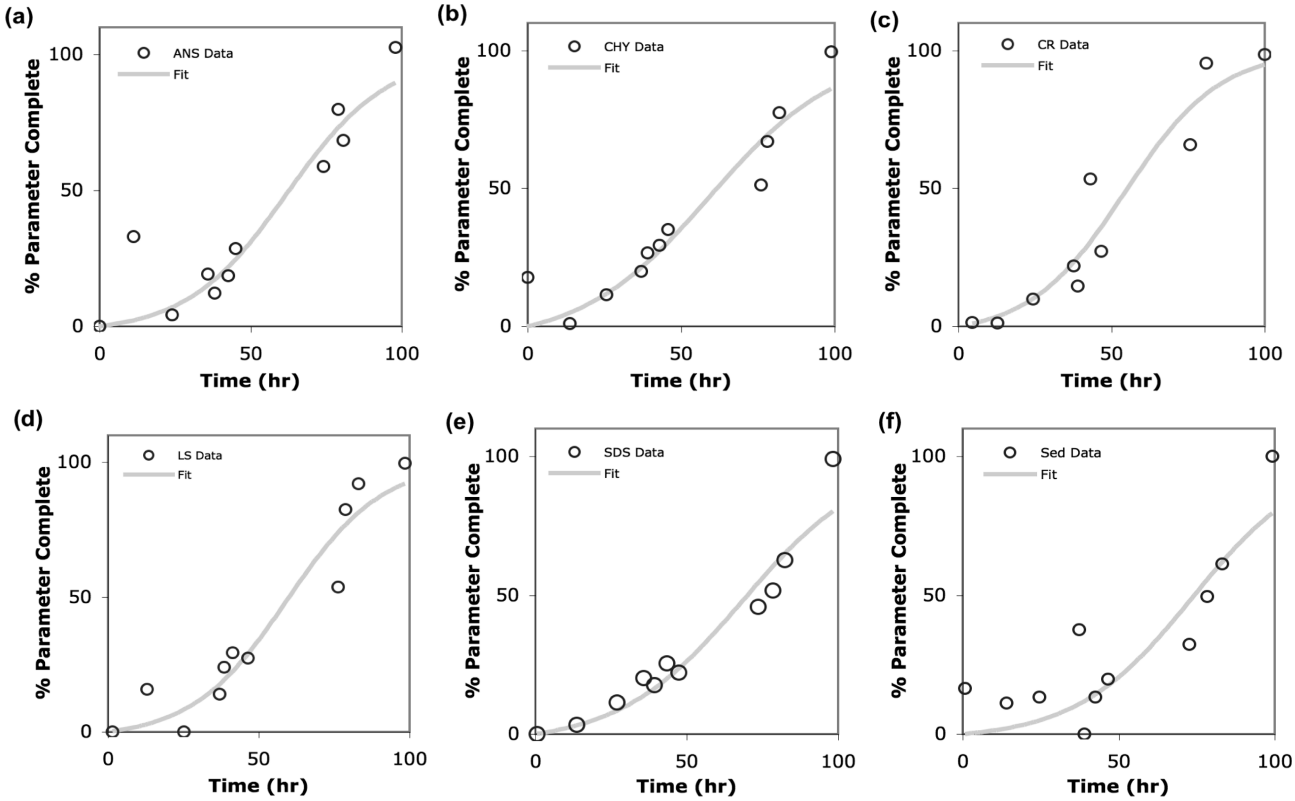


FIGURE 1: Aggregation of Sup35p measured by Lindquist and co-workers (*23*) using six different physical methods. Specifically, Sup35p aggregation was assessed by (a) ANS fluorescence, (b) chymotrypsin resistance, (c) Congo Red, (d) light scattering, (e) SDS−PAGE, and (f) sedimentation methods. Each data set was digitized and fit using the F−W model. Table 2 shows the $k_1$ and $k_2$ rate constants obtained for parts a−f. The important finding is that the $k_1$ values, as well as the $k_2$ values, are all equal to one another within experimental error for the six techniques used.

In eq 1, $[B]_t$ represents the concentration of aggregated protein at time $t$ (vide infra), $[A]_0$ represents the initial protein concentration, and $k_1$ and $k_2$ are the aforementioned rate constants for nucleation and growth, respectively.

In each of the fits presented herein and as previously detailed (*31*), we have by necessity assumed (as generally done in the literature) that (i) all forms of kinetic measurement are directly proportional to the percent of aggregated protein (i.e., that the physical method used is a direct measure of the aggregated protein) and (ii) the data are ideal; that is, only the aggregated protein is responsible for the observed signal. Furthermore, where noted in the cases that follow, the published data sets were normalized to an initial minimum of zero.

## RESULTS

In what follows, we present fits of 24 representative yeast prion aggregation kinetic data sets, including the yeast prions Sup35p, Ure2p, and Rnq1p, as well as three representative mammalian (both mouse and human) prion aggregation kinetic data sets. Each data set was fit using the F−W model; the results are displayed in Figures 1−10 and summarized in Table 3.

*Fitting Yeast Prion Aggregation Kinetic Data.* Figures 1−8 show representative kinetic data sets for yeast prion aggregation fit using the F−W model from the three yeast prion systems Sup35p, Ure2p, and Rnq1p. To start, we looked at Sup35p aggregation kinetic data obtained by Lindquist and co-workers using six different physical methods (*23*). Displayed in Figure 1 are the F−W fits to each set of aggregation kinetic data measured by ANS, chymotrypsin resistance, Congo Red binding, light scattering, SDS−PAGE, and sedimentation. Interestingly, and as displayed in Table 2, each of these physical methods gives the same nucleation ($k_1$) and growth ($k_2$) rate constants within experimental error. However, one issue with the data sets shown in Figure 1 is that the spectra appear to be somewhat noisy, resulting in relatively large error bars in the rate constants and in lower than desired coefficients of determination ($R^2$, Table 2). Nevertheless, Lindquist and co-workers are the first (to the best of our knowledge) to perform this important control of examining protein aggregation kinetic data with at least six physical methods. Our analysis herein is the first to deconvolute that data into $k_1$ and $k_2$ values showing that both rate constants are the same within experimental error with all methods used, at least for the Sup35p system.

Table 2: Rate Constants and Coefficients of Determination ($R^2$) Obtained from the Fits Shown in Figure 1 Measuring the Aggregation of Sup35p by the Six Listed Methods

| physical method | $k_1$ ($h^{-1}$) | $k_2$ ($\mu M^{-1}$ $h^{-1}$) | $R^2$ [a] |
|---|---|---|---|
| ANS fluorescence (ANS) | $1(1) \times 10^{-3}$ | $1.2(2) \times 10^{-2}$ | 0.88158 |
| chymotrypsin resistance (CHY) | $3(1) \times 10^{-3}$ | $1.0(2) \times 10^{-2}$ | 0.91165 |
| Congo Red (CR) | $2(1) \times 10^{-3}$ | $1.2(4) \times 10^{-2}$ | 0.91684 |
| light scattering (LS) | $1.4(8) \times 10^{-3}$ | $1.2(2) \times 10^{-2}$ | 0.92883 |
| SDS−PAGE (SDS) | $1.7(8) \times 10^{-3}$ | $0.9(2) \times 10^{-2}$ | 0.93344 |
| sedimentation (Sed) | $1(1) \times 10^{-3}$ | $1.0(4) \times 10^{-2}$ | 0.76354 |

[a] The coefficient of determination ($R^2$); the closer the value of $R^2$ is to 1, the more precise the fit is to the data.

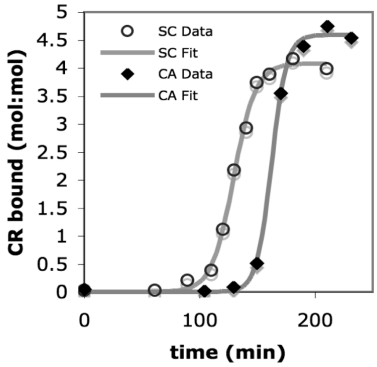


FIGURE 2: Weissman and co-workers' aggregation of Sup35p PrDM from different yeast species, measured by Congo Red binding at 2.5 $\mu$M PrD with continuous rotation (*32*). The data sets were digitized, normalized to an initial minimum of zero, and then fit to the F−W model. Resultant rate constants for *SC*: $k_1 = 1(1) \times 10^{-7}$ $\text{min}^{-1}$ [$k_1 = 6(6) \times 10^{-6}$ $\text{h}^{-1}$], and $k_2 = 4.2(4) \times 10^{-2}$ $\mu\text{M}^{-1}$ $\text{min}^{-1}$ [$k_2 = 2.5(2)$ $\mu\text{M}^{-1}$ $\text{h}^{-1}$] ($R^2 = 0.997$). Resultant rate constants for *CA*: $k_1 = 2(9) \times 10^{-12}$ $\text{min}^{-1}$ [$k_1 = 1(5) \times 10^{-10}$ $\text{h}^{-1}$], and $k_2 = 6(1) \times 10^{-2}$ $\mu\text{M}^{-1}$ $\text{min}^{-1}$ [$k_2 = 3.6(6)$ $\mu\text{M}^{-1}$ $\text{h}^{-1}$] ($R^2 = 0.998$). The relatively large error bars in $k_1$ result from the lack of data around the initial, concave portion of the sigmoidal curve.

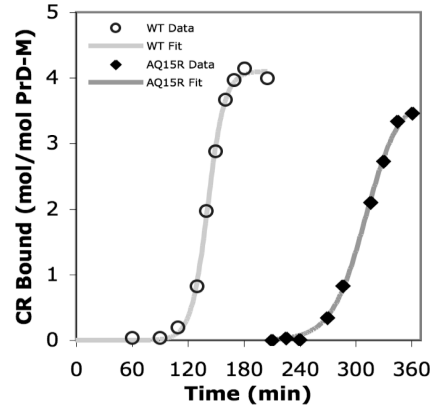


FIGURE 3: Weissman and co-workers' Sup35p and mutant AQ15R digitized aggregation data measured by Congo Red binding (*33*). The digitized data were normalized to an initial minimum of zero and then fit using the F−W model. Resultant rate constants for the WT: $k_1 = 2(2) \times 10^{-8}$ $\text{min}^{-1}$ [$k_1 = 1(1) \times 10^{-6}$ $\text{h}^{-1}$], and $k_2 = 4.5(3) \times 10^{-2}$ $\mu\text{M}^{-1}$ $\text{min}^{-1}$ [$k_2 = 2.7(2)$ $\mu\text{M}^{-1}$ $\text{h}^{-1}$] ($R^2 = 0.999$. Resultant rate constants for AQ15R: $k_1 = 2(2) \times 10^{-9}$ $\text{min}^{-1}$ [$k_1 = 1(1) \times 10^{-7}$ $\text{h}^{-1}$], and $k_2 = 2.1(1) \times 10^{-2}$ $\mu\text{M}^{-1}$ $\text{min}^{-1}$ [$k_2 = 1.26(6)$ $\mu\text{M}^{-1}$ $\text{h}^{-1}$] ($R^2 = 0.999$). Here, again, the relatively large error bars in $k_1$ result from the lack of data around the initial, concave portion of the sigmoidal curve.

Another Sup35p data set we examined comes from the studies of Weissman and co-workers (*32*). Those authors looked at whether the prion function of Sup35p is conserved in distantly related yeasts by expressing foreign prion domains (PrD) of Sup35p in *SC* (*32*). The authors found that the prion function of Sup35p was conserved among these yeasts. The ability to form amyloid fibrils in vitro was also conserved as illustrated in Figure 2, which includes fits by the F−W model (*32*).[2] From the F−W fits in Figure 2, prion aggregation of Sup35p from the yeast species *SC* and *Candida albicans* (*CA*) display (i) different nucleation kinetics, as shown by $k_1$ values that appear to differ by 5 orders of magnitude (note, however, that there are large error bars in these $k_1$ values[3]), but (ii) similar growth kinetics, as demonstrated by $k_2$ values that are on the same order of magnitude.

The third literature study we examined is an interesting paper by Weissman and co-workers in which they used a genetic screening technique to identify mutations that cause defects in the amyloid formation of Sup35p (*33*). Visual examination of the aggregation curves shown in Figure 3 for WT Sup35p and a Q15R mutant (where Q at position 15 is substituted with R) reveals that the induction period is lengthened, qualitatively, on going from the WT to the mutant. Using the F−W model, we were able to more quantitatively dissect the data. Specifically, we find that the mutation (i) does affect nucleation kinetics, decreasing the observed $k_1$ value by 1 order of magnitude on going from the WT to the mutant (although here, again, large error bars in $k_1$ values are present[3]) while (ii) the growth kinetics are less affected, with the $k_2$ value for the mutant being approximately one-half of that for the WT.

In a different study in 1999, Lindquist and co-workers examined the importance of oligopeptide repeat expansions in Sup35p (*34*). To investigate this idea, they created the variants RΔ2−5 and R2E2 in which RΔ2−5 differs from the WT in that it has the last four repeats deleted while R2E2 has two additional copies of the second repeat. Via the F−W fits to their aggregation data shown in Figure 4a, we now can look at the effect of repeat expansion or deletion on nucleation and growth, separately. The fits reveal that no statistically significant trend due to the effect of repeat sequences on nucleation is observed (Figure 4b). (Although the $k_1$ values appear to be increased by 1 order of magnitude for both the deletion and repeat expansion variants as compared to that of the WT,[4] the large error bars render the results statistically equivalent.[3]) On the other hand, the repeat sequences do appear to affect the growth kinetics, as shown by the increase in $k_2$ values with an increasing number of repeat sequences (Figure 4c). These observations are consistent with Osherovich et al.'s findings of residues 1−39 of Sup35p driving in vivo prion formation and residues 40−114 driving prion propagation (*35*). These are valuable insights into the factors affecting nucleation versus growth that were previously buried within this interesting 1999 study (*34*).

The next interesting study that caught our eye was the investigation by Perrett and co-workers of the role of specific glutamine/asparagine (Gln/Asn) rich regions, contained in

[2] The authors also found that a species barrier inhibited prion induction by Sup35p from different species. That is, "foreign" PrDs could not efficiently seed prion formation by "wild-type" Sup35p (but foreign PrDs did behave as prions themselves). We chose not to fit cross-seeding experiments in this data set, as seeding introduces B into the reaction mixture, which then is not be properly modeled by eq 1. [We have, however, provided an equation elsewhere (*31*) that can in principle deal with seeded data sets.] To the best of our knowledge, no data set treated herein involves any type of seeding.

[3] Ideal data sets would have more data points around the concave portion of the sigmoidal curve, to minimize error bars from the fit, especially the error in $k_1$.

[4] We have observed that the (inverse of the) induction period is an indicator of nucleation kinetics only when the sigmoidal aggregation curve is not "rounded" (i.e., when the initial portion of the curve is flat and there is a clear-cut transition to the linear slope portion). When the sigmoidal curve is rounded (i.e., when the initial portion of the curve is not flat and the transition to the linear slope portion shows a wide concave angle), we find that both nucleation and growth kinetics are strongly convoluted in the induction period. Additional studies on this issue are in progress.

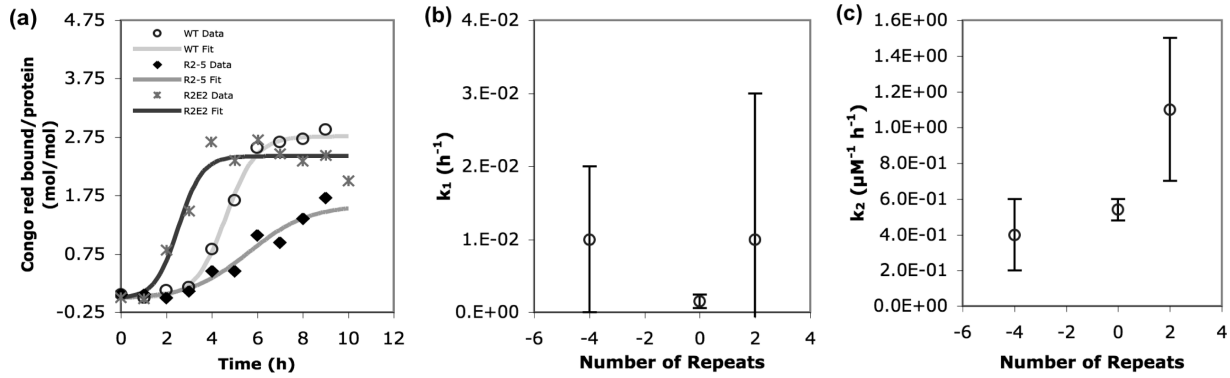


FIGURE 4: (a) Aggregation data for WT Sup35p along with mutants, RΔ2−5 and R2E2, measured by Congo Red from Lindquist and co-workers (*34*). Note that "number of repeats" in panels b and c is really the *difference* in the number of repeats. The RΔ2−5 mutant contains four fewer repeat sequences than the WT, while R2E2 has two more repeat sequences (*34*). The data were digitized, normalized to an initial minimum of zero, and fit by the F−W model. The following rate constants were obtained: for WT, $k_1 = 1.5(9) \times 10^{-3}$ h$^{-1}$ and $k_2 = 5.4(6) \times 10^{-1}$ $\mu$M$^{-1}$ h$^{-1}$ ($R^2 = 0.995$); for RΔ2−5, $k_1 = 1(1) \times 10^{-2}$ h$^{-1}$ and $k_2 = 4(2) \times 10^{-1}$ $\mu$M$^{-1}$ h$^{-1}$ ($R^2 = 0.945$); for R2E2, $k_1 = 1(2) \times 10^{-2}$ h$^{-1}$ and $k_2 = 1.1(4)$ $\mu$M$^{-1}$ h$^{-1}$ ($R^2 = 0.951$). (b and c) Correlations between the difference in the number of repeat sequences (set to zero for WT) and the $k_1$ and $k_2$ values obtained from the data fits in panel a.

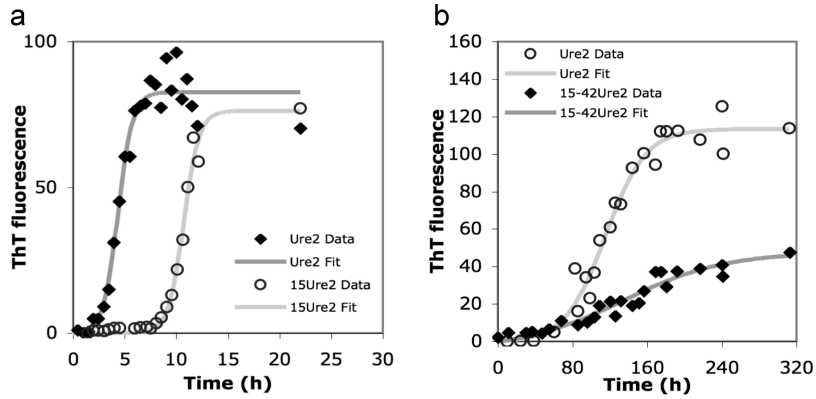


FIGURE 5: (a) Perrett and co-workers' 40 $\mu$M Ure2p and mutant 15Ure2 aggregation data measured by fluorescence, at pH 7.5 and 25 °C, with shaking (*36*). The data were digitized, normalized to an initial minimum of zero, and then fit using the F−W model. Rate constants for Ure2p: $k_1 = 3(2) \times 10^{-3}$ h$^{-1}$, and $k_2 = 4.1(7) \times 10^{-2}$ $\mu$M$^{-1}$ h$^{-1}$ ($R^2 = 0.975$). Rate constants for 15Ure2: $k_1 = 1(1) \times 10^{-6}$ h$^{-1}$, and $k_2 = 3.3(4) \times 10^{-2}$ $\mu$M$^{-1}$ h$^{-1}$ ($R^2 = 0.999$). (b) Digitized data of Perrett and co-workers' 40 $\mu$M Ure2p and mutant Δ15−42Ure2 aggregation data measured by fluorescence, at pH 9 and 4 °C, without shaking (*36*). The data were fit to the F−W model. Resultant rate constants for Ure2p: $k_1 = 2(1) \times 10^{-4}$ h$^{-1}$, and $k_2 = 1.3(2) \times 10^{-3}$ $\mu$M$^{-1}$ h$^{-1}$ ($R^2 = 0.975$). Resultant rate constants for Δ15−42Ure2: $k_1 = 1.4(4) \times 10^{-3}$ h$^{-1}$, and $k_2 = 4(1) \times 10^{-4}$ $\mu$M$^{-1}$ h$^{-1}$ ($R^2 = 0.931$).

residues 1−14 and 42−90, of the prion domain of Ure2p (*36*). We re-examined the aggregation data shown in Figure 5 for both WT and mutant Ure2p, using the F−W model to obtain quantitative $k_1$ and $k_2$ rate constants. For the mutant 15Ure2 (Figure 5a), which refers to Ure2p with residues 1−14 removed (a Gln/Asn rich region), the nucleation kinetics are strongly affected, as shown by a $k_1$ value decreased by 3 orders of magnitude as compared to that of WT (where this difference is beyond the fitting error). On the other hand, the mutation has little effect on growth kinetics, with $k_2$ values being the same within experimental error. Consistent with these observations is the previous work addressing nucleation and showing that deletion of residues 2−14 of Ure2p dramatically reduces the in vivo frequency with which new prions are detected (*37*). For the mutant Δ15−42Ure2 (Figure 5b), which refers to Ure2p with residues 15−42 removed (a region less enriched with Gln/Asn), the authors note a strong effect on the intensity of the fluorescence signal and hypothesize that the less enriched Gln/Asn region which was removed might be a binding site for ThT (*36*). As a consequence, it is not clear at present whether the change in the mutant aggregation curve (and its F−W fit) actually represents different aggregation kinetics or if it is some type of experimental artifact. The deconvolution of $k_1$ and $k_2$ is, however, useful in directing needed future control experiments.

Perrett and co-workers also looked at the stability of folding intermediates of Ure2p and studied the effect of experimental variables on its aggregation (*38*). The effect of varying Ure2p concentration is shown in Figure 6, along with fits to the F−W model. [Unfortunately, the full range of concentrations could not be digitized or fit, since at lower concentrations the aggregation curves (in their published form) were convoluted in the early portion of the curve, that early portion being crucial in determining the nucleation kinetics (*38*).] In Figure 7, we show four representative examples of the effect of pH and temperature on the aggregation of Ure2p, along with fits by the F−W model (*38*). In this case, all the published curves could be digitized. However, some of the curves differed significantly enough from the average curve obtained under the same conditions (as the results summarized in Table 4 of ref *38* indicate) that we chose not to attempt to draw trends (*38*). The main conclusions from the data and fits in Figure 7, then, are (i) the F−W model fits the data well, but (ii) more precise data would be useful for drawing correlations for different

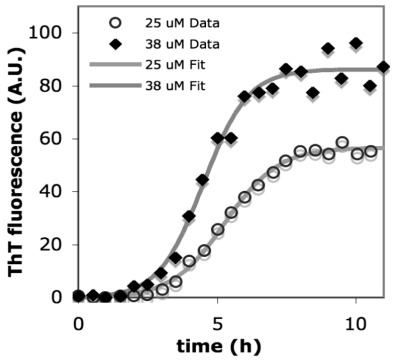


FIGURE 6: Perrett and co-workers' Ure2p aggregation measured by ThT fluorescence for different Ure2p concentrations at pH 7.5 and 25 °C, in 50 mM Tris buffer with shaking (*38*). The data were digitized, normalized to an initial minimum of zero, and then fit by the F−W model. Resultant rate constants for 25 $\mu$M Ure2p: $k_1 = 4.2(9) \times 10^{-3}$ h$^{-1}$, and $k_2 = 4.2(2) \times 10^{-2}$ $\mu$M$^{-1}$ h$^{-1}$ ($R^2 = 0.997$). Resultant rate constants for 38 $\mu$M Ure2p: $k_1 = 5(2) \times 10^{-3}$ h$^{-1}$, and $k_2 = 3.3(3) \times 10^{-2}$ $\mu$M$^{-1}$ h$^{-1}$ ($R^2 = 0.987$).

concentrations of prion protein, varying temperatures, and varying pH values.

In a study aimed at demonstrating a protein-only mechanism of infection for [*PIN*+], Liebman and co-workers used a Glu/Asn rich recombinant fragment of Rnq1p (residues 132−405) that polymerizes into fibrils (*12*). The authors studied the effect of agitation, concentration, and temperature on the Rnq1p-(132−405) aggregation curves measured by continuous ThT fluorescence. We show one representative example of Rnq1p-(132−405) aggregation in Figure 8, fit by the F−W model. [Unfortunately, most of the published curves could not be readily digitized (*12*).] The primary conclusion from Figure 8 is that the observed data are well fit by the F−W two-step kinetic model.

*Fitting Mammalian Prion Aggregation Kinetic Data.* Figures 9 and 10 show representative data sets of mammalian prion aggregation curves fit using the F−W model, for both mouse and human prion systems. Cohen and co-workers (*39*) were interested in the mechanism of conversion of the (monomeric, α-helical) cellular form of the prion protein, $PrP^C$, into its (polymeric, $\beta$-sheet) prion form, $PrP^{Sc}$; hence, they collected kinetic data for the aggregation of recombinant mouse prion protein (MoPrP). The aggregation curve is shown in Figure 9, illustrating the good fit of the F−W nucleation and growth model.

Next, we looked at Baskakov and co-workers' study of the aggregation of recombinant human prion protein (HuPrP) under different experimental conditions, including various prion protein concentrations (*40*). Two aggregation curves illustrating the effect of HuPrP concentration are shown in Figure 9, along with fits to the F−W model. Here, again, the full range of concentrations could not be digitized or fit by us, since at lower concentrations the published aggregation curves were convoluted in the early portion of the curve (*40*). The fits that were possible are quite good, indicating that it would be of interest to investigate other concentrations of HuPrP.

*Addressing the Issue of the Effects of Agitation.* To address the issue of agitation (and resulting fragmentation) on prion aggregation, we searched the literature for prion kinetic data sets of a system under the same experimental conditions, with and without agitation. Only one unseeded data set was found that could be readily digitized; this data set and its analysis can be found in the Supporting Information. Unfortunately, the likely presence of several possible experimental issues in this otherwise important data set kept us from being able to properly address the important issue of fragmentation. In the future we plan to obtain our own data sets to address this issue via the F−W model (*41*).

Table 3 summarizes the 24 representative cases of yeast prion and three representative cases of mammalian prion aggregation kinetics that were successfully curve-fit using the F−W model (Figures 1−10). Of course, anytime one goes to the trouble to collect and tabulate this amount of data, the resultant table merits scrutiny for any insights or needed future experiments suggested by the data and the cross comparisons. A couple of such comparisons in Table 3 caught our eye; the reader is encouraged to find their own, within the caveats noted below of the issues involved in comparing different systems and different experimental conditions. (i) A comparison of data for ostensibly similar systems (e.g., entries 3 and 9) yields $k_1$ values differing by $\sim 10^3$ and $k_2$ values differing by $\sim 10^2$. Hence, repeats of identical systems under identical (as well as a broader range of) conditions, and in multiple laboratories, remain to be done to determine what $k_1$ and $k_2$ values (and what level of reproducibility) results. Especially important is the fact that (ii) considerable caution needs to be exercised in any such cross comparisons, even for identical proteins since rate constants can be sensitive to the precise experimental conditions just like any other physical constant of a system. Indeed, Table 3 is just the first such table of its kind, so there is a need for many more $k_1$ and $k_2$ values obtained under carefully controlled and reported conditions.

## DISCUSSION

*Additional Background on the Two-Step F−W Model.* The F−W model has been shown to apply to a variety of aggregation processes in nature, including (first) nanocluster formation (*42*−*47*) and more recently protein fibrillation (*31*). It consists, typically, of slow nucleation followed by fast autocatalytic growth, as displayed in Scheme 1, where $k_1$ and $k_2$ represent the rate constants for nucleation and growth, respectively. In the case of protein aggregation, A corresponds to a monomeric form of the protein while B corresponds to the protein in oligomers that are past the nucleation stage. As species B is both a product and a catalyst for growth, the second step of the F−W model is termed autocatalytic (the strict kinetic definition of autocatalysis being A + B → 2B).

The F−W model results from the use of the concept of pseudoelementary kinetics, an approach pioneered in the 1970s by R. Noyes (*48*). With this approach, the many substeps involved in nucleation and growth are combined into two pseudoelementary steps of nucleation and growth, which behave kinetically as (pseudo) elementary steps.[5] The two pseudoelementary steps of nucleation and growth in the F−W model yield an integrable rate equation (eq 1) which can be used to fit concentrations as a function of time, as

[5] The pseudoelementary step concept involves summing faster reactions with one or more slower reactions, giving an overall (sum) reaction that can be treated kinetically as an elementary step.

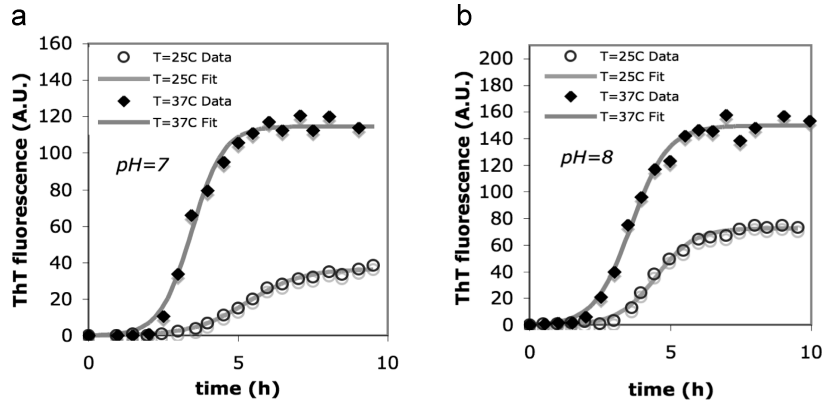


FIGURE 7: (a) Perrett and co-workers' Ure2p aggregation measured by ThT fluorescence for different temperatures at pH 7 and 30 $\mu$M Ure2p, in 50 mM phosphate buffer with shaking (*38*). The data were digitized, normalized to an initial minimum of zero, and then fit to the F−W model. Resultant rate constants for 25 °C: $k_1 = 3.2(9) \times 10^{-3}$ h$^{-1}$, and $k_2 = 3.7(3) \times 10^{-2}$ $\mu$M$^{-1}$ h$^{-1}$ ($R^2 = 0.996$). Resultant rate constants for 37 °C: $k_1 = 3(1) \times 10^{-3}$ h$^{-1}$, and $k_2 = 6.3(7) \times 10^{-2}$ $\mu$M$^{-1}$ h$^{-1}$ ($R^2 = 0.992$). (b) Perrett and co-workers' Ure2p aggregation measured by ThT fluorescence for different temperatures at pH 8 and 30 $\mu$M Ure2p, in 50 mM phosphate buffer with shaking (*38*). The data were digitized, normalized to an initial minimum of zero, and then fit to the F−W model. Resultant rate constants for 25 °C: $k_1 = 1.8(7) \times 10^{-3}$ h$^{-1}$, and $k_2 = 5.0(4) \times 10^{-2}$ $\mu$M$^{-1}$ h$^{-1}$ ($R^2 = 0.995$). Resultant rate constants for 37 °C: $k_1 = 6(2) \times 10^{-3}$ h$^{-1}$, and $k_2 = 5.1(5) \times 10^{-2}$ $\mu$M$^{-1}$ h$^{-1}$ ($R^2 = 0.993$).

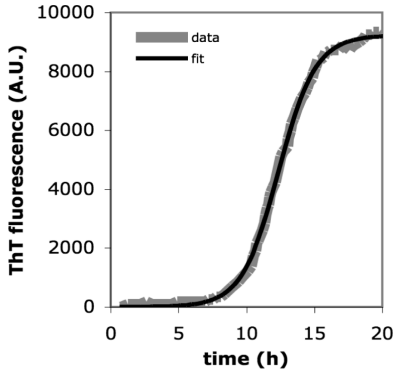


FIGURE 8: Liebman and co-workers' aggregation of Rnq1p-(132−405) measured by continuous ThT fluorescence at 27 °C and 110 $\mu$M Rnq1p-(132−405), with agitation (*12*). The data were digitized and fit to the F−W model. Resultant rate constants: $k_1 = 8.0(9) \times 10^{-5}$ h$^{-1}$, and $k_2 = 6.7(1) \times 10^{-3}$ $\mu$M$^{-1}$ h$^{-1}$ ($R^2 = 0.999$).

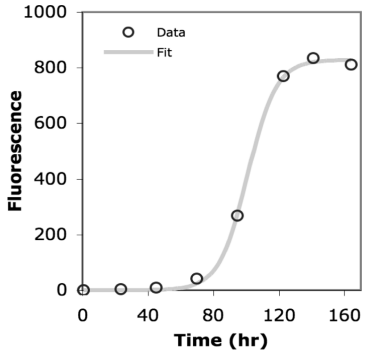


FIGURE 9: Digitized data for the assembly of 40 $\mu$M MoPrP from Cohen and co-workers normalized to an initial minimum of zero and then fit using the F−W model (*39*). Resultant rates constants: $k_1 = 1(1) \times 10^{-6}$ h$^{-1}$, and $k_2 = 2.9(2) \times 10^{-3}$ $\mu$M$^{-1}$ h$^{-1}$ ($R^2 = 0.999$).

shown here and elsewhere (*31, 42*−*47*). The resulting rate constants $k_1$ and $k_2$ for nucleation and growth, respectively, can thus be seen as pseudoelementary rate constants (i.e., where $k_1$ and $k_2$ are pseudoelementary step "rate constants" that may vary with concentration and, therefore, may not be true "constants").

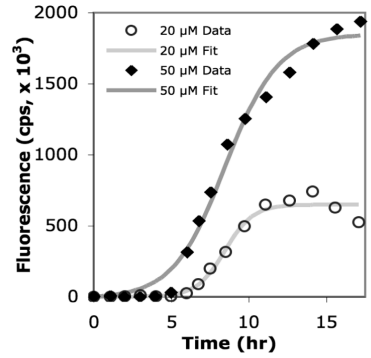


FIGURE 10: Baskakov and co-workers' kinetics of the human recombinant prion protein (Hu rPrP 90−231) digitized data from varying concentrations normalized to an initial minimum of zero and then fit to the F−W model (*40*). The following rate constants and $R^2$ values were obtained: for 20 $\mu$M, $k_1 = 1(2) \times 10^{-4}$ h$^{-1}$ and $k_2 = 5(1) \times 10^{1}$ $\mu$M$^{-1}$ h$^{-1}$ ($R^2 = 0.977$); 50 $\mu$M, $k_1 = 4(2) \times 10^{-3}$ h$^{-1}$ and $k_2 = 1.2(2) \times 10^{1}$ $\mu$M$^{-1}$ h$^{-1}$ ($R^2 = 0.988$).

Because of the convolution of many steps into (kinetically useful) average $k_1$ and $k_2$ steps, the F−W model *is at best a starting point in attempts to elucidate the molecular picture of the aggregation process*.[6] The primary use of the F−W two-step kinetic model is to deconvolute (average) nucleation from (average) growth. It is obviously a minimalistic kinetic model, and its limitations (vide infra) derive from that Ockham's razor nature.

*Fitting Prion Aggregation Data with the F−W Model: Effect of the N-Terminal and C-Terminal Regions of the Sup35p Prion Domain on Nucleation and Growth.* The prion domain (PrD) of the yeast prion protein Sup35p consists of

[6] An alternative form of the model, which provides more physical insight, is shown below, where B is replaced by the "full oligomer" $B_n$. This descriptive form does not, however, allow for a simple mathematical treatment with analytically integrable rate equations. As such, it cannot be easily used to fit experimental aggregation kinetic data.

$$n\,A \xrightarrow{k_1'} B_n$$

$$A + B_n \xrightarrow{k_2'} B_{n+1}$$

Table 3: Rate constants and coefficients of determination ($R^2$) from fitting 27 prion aggregation kinetic data sets to the F−W 2-step model

| entry | ref | system | distinguishing experimental details | data collection method | $k_1$[a] ($h^{-1}$) | $k_2$[a,b] ($\mu M^{-1}$ $h^{-1}$) | $R^2$ [c] |
|---|---|---|---|---|---|---|---|
| 1 | Lindquist (*23*) | Sup35p | | ANS | $1(1) \times 10^{-3}$ | $1.2(2) \times 10^{-2}$ | 0.882 |
| 2 | | | | CHY | $3(1) \times 10^{-3}$ | $1.0(2) \times 10^{-2}$ | 0.912 |
| 3 | | | | CR | $2(1) \times 10^{-3}$ | $1.2(4) \times 10^{-2}$ | 0.917 |
| 4 | | | | LS | $1.4(8) \times 10^{-3}$ | $1.2(2) \times 10^{-2}$ | 0.929 |
| 5 | | | | SDS | $1.7(8) \times 10^{-3}$ | $9(2) \times 10^{-3}$ | 0.933 |
| 6 | | | | Sed | $1(1) \times 10^{-3}$ | $1.0(4) \times 10^{-2}$ | 0.764 |
| 7 | Weissman (*32*) | Sup35p | from *SC* | CR | $6(6) \times 10^{-6}$ | 2.5(2) | 0.997 |
| 8 | | | from *CA* | CR | $1(5) \times 10^{-10}$ | 3.6(6) | 0.998 |
| 9 | Weissman (*33*) | Sup35p | WT | CR | $1(1) \times 10^{-6}$ | 2.7(2) | 0.999 |
| 10 | | | AQ15R | CR | $1(1) \times 10^{-7}$ | 1.26(6) | 0.999 |
| 11 | Lindquist (*34*) | Sup35p | WT | CR | $1.5(9) \times 10^{-3}$ | $5.4(6) \times 10^{-1}$ | 0.995 |
| 12 | | | RΔ2−5 | CR | $1(1) \times 10^{-2}$ | $4(2) \times 10^{-1}$ | 0.946 |
| 13 | | | R2E2 | CR | $1(2) \times 10^{-2}$ | 1.1(4) | 0.951 |
| 14 | Perrett (*36*) | Ure2p | Ure2 agitated | ThT | $3(2) \times 10^{-3}$ | $4.1(7) \times 10^{-2}$ | 0.975 |
| 15 | | | 15Ure2 agitated | ThT | $1(1) \times 10^{-6}$ | $3.3(4) \times 10^{-2}$ | 0.999 |
| 16 | | | Ure2 nonagitated | ThT | $2(1) \times 10^{-4}$ | $1.3(2) \times 10^{-3}$ | 0.975 |
| 17 | | | Δ15−42Ure2 nonagitated | ThT | $1.4(4) \times 10^{-3}$ | $4(1) \times 10^{-2}$ | 0.931 |
| 18 | Perrett (*38*) | Ure2p | 25 μM | ThT | $4.2(9) \times 10^{-3}$ | $4.2(2) \times 10^{-2}$ | 0.997 |
| 19 | | | 38 μM | ThT | $5(2) \times 10^{-3}$ | $3.3(3) \times 10^{-2}$ | 0.987 |
| 20 | | | pH 7, 25 °C | ThT | $3.2(9) \times 10^{-3}$ | $3.7(3) \times 10^{-2}$ | 0.996 |
| 21 | | | pH 7, 37 °C | ThT | $3(1) \times 10^{-3}$ | $6.3(7) \times 10^{-2}$ | 0.992 |
| 22 | | | pH 8, 25 °C | ThT | $1.8(7) \times 10^{-3}$ | $5.0(4) \times 10^{-2}$ | 0.995 |
| 23 | | | pH 8, 37 °C | ThT | $6(2) \times 10^{-3}$ | $5.1(5) \times 10^{-2}$ | 0.993 |
| 24 | Liebman (*12*) | Rnq1p | | ThT | $8.0(9) \times 10^{-5}$ | $6.7(1) \times 10^{-3}$ | 0.999 |
| 25 | Cohen (*39*) | mouse prion | | ThT | $1(1) \times 10^{-6}$ | $2.9(2) \times 10^{-3}$ | 0.999 |
| 26 | Baskakov (*40*) | human prion | 20 μM | ThT | $1(2) \times 10^{-4}$ | $5(1) \times 10^{1}$ | 0.977 |
| 27 | | | 50 μM | ThT | $4(2) \times 10^{-3}$ | $1.2(2) \times 10^{1}$ | 0.988 |

[a] The error bars are for the fit and are determined by the square root of the reduced $\chi^2$ based on a modified Levenberg−Marquardt algorithm. [b] The concentration units for $k_2$ were determined by multiplying by the maximum intensity and dividing by the initial starting concentration of the respective protein being measured. [c] The coefficient of determination ($R^2$).

two subdomains: (i) the N-terminal portion (amino acids 1−39), which is rich in glutamine/asparagine (Gln/Asn) residues and is thought to drive prion aggregation (*35*), and (ii) the C-terminal region (amino acids 40−114), which contains a series of imperfect oligopeptide repeats and is believed to play a role in prion propagation. Experiments with both Sup35p and Ure2p prion proteins have demonstrated that it is the overall amino acid composition (rather than the sequence) of the prion domain that is the predominant feature driving prion formation (*37, 49*).

Among yeast species, the overall composition of the prion domain of Sup35p is relatively similar. Little homology in sequence is found for the N-terminal portion of PrD, but the amino acid composition is generally conserved, whereas in the C-terminal portion of PrD, both the amino acid composition and the overall repeat structure (thus the sequence) are generally conserved among species. Figure 2 (vide supra) shows aggregation curves obtained by Weissman and co-workers for the prion domain of Sup35p from *SC* and *CA* yeast species (*32*). Fits by the F−W model indicate that while nucleation kinetics (i.e., values of the nucleation rate constant $k_1$) vary considerably between species, growth kinetics (and the growth rate constant $k_2$) vary much less. Since the main difference between the prion domains of these yeast species lies in the sequence of the N-terminal portion, our results suggest the hypothesis that the N-terminal portion of the PrD in Sup35p affects nucleation more than growth, an observation consistent with the previous findings of Osterovish et al. (*35*).

When Weissman and co-workers screened the prion domain of Sup35p to look for mutations causing defects in amyloid formation, they found that (i) all these mutations were contained within a short region between residues 8 and 24 (a region with a high content of Gln and Asn residues) and (ii) most mutations were the result of a Gln or Asn mutation (*33*). Therefore, the authors suspected "a critical role for [the] Gln and Asn residues" in the N-terminal portion of the Sup35p PrD (*33*). Figure 3 shows the aggregation curves measured for the variants wild type (WT) and Q15R mutant (with Q → R at position 15) (*33*). Fits by the F−W model show that the mutation resulted in appreciably slower nucleation ($k_1$) kinetics, and in somewhat slower growth ($k_2$) kinetics. Since the mutation involved only substituting a glutamine (Q) with arginine (R) at position 15, our results indicate that the (Gln/Asn rich) N-terminal portion of the PrD in Sup35p affects nucleation kinetics more than growth kinetics. These results are also consistent with subsequent single-fiber growth studies, which indicate that the Q15R mutant exhibits average growth kinetics similar to those of WT (*50*). The results also allow an intriguing prediction that merits future testing: although the Q15R mutant does not efficiently add to WT prion fibers in vivo (*33*), when expressed as the sole copy of Sup35p, the Q15R mutant should have a low frequency of prion formation but should still be able to efficiently propagate prions once they form. It should be noted that this mutant was isolated on the basis of its inability to propagate wild-type [*PSI*+]. However, this may reflect a species barrier between WT and Q15R rather than the intrinsic ability of Q15R to propagate prions.

The significance with respect to prion aggregation of oligopeptide repeat sequences, located in the C-terminal portion of the Sup35p prion domain, came into focus when Lindquist and co-workers created variants of Sup35p that differed only in the number of repeats (*34*). Figure 4a (vide supra) shows the aggregation curves obtained for Sup35p WT, a deletion variant RΔ2−5 (with repeats 2−5 deleted), and an expansion variant R2E2 (with repeat 2 expanded twice). Fits by the F−W model suggest that the number of

repeats affects growth kinetics, as indicated by a correlation between values of the growth rate constant $k_2$ and the (difference in) number of repeats (Figure 4c). On the other hand (in part due to large error bars), we could not detect a reliable correlation between the nucleation rate constant $k_1$ and the (difference in) number of repeats (Figure 4b). Since the variants differed in the number of oligopeptide repeat sequences, our analysis suggests the hypothesis that the (repeats-containing) C-terminal portion of the PrD in Sup35p plays a role that affects growth kinetics, an observation consistent with the proposed role of the repeats in prion propagation (*35*).

*Fitting Prion Aggregation Data with the F−W Model: Effect of a Gln/Asn Rich Region of the Ure2p Prion Domain on Nucleation and Growth.* The prion domain of Ure2p (residues 1−90) shows consistently a high Gln/Asn content. As there is no evidence of separate aggregation or propagation subdomains, the Ure2p PrD is generally not subdivided. Perrett and co-workers were interested in the role of specific regions of the Ure2p PrD that are particularly rich in Gln and Asn and created a 15Ure2 mutant with residues 1−14 (a Gln/Asn rich region) removed (*36*). Figure 5a, vide supra, shows aggregation curves measured for the WT and 15Ure2 variants. Fits by the F−W model indicate that the mutant displays substantially slower nucleation ($k_1$) kinetics, but rather similar growth ($k_2$) kinetics. Because the mutation results from the removal of a Gln/Asn rich region, our results suggest the hypothesis that this Gln/Asn rich region in the PrD of Ure2p plays a role that affects nucleation kinetics more than growth kinetics (*37*). Further tests of this and the other hypotheses provided above are, of course, needed.

*A Return to the Issue of Fragmentation.* We began these studies expecting that the F−W two-step model would *not* be able to fit prion aggregation kinetic data due to the fact that it does not specifically account for fragmentation step(s), yet fragmentation is generally believed to be an integral part of prion aggregation (*51*−*55*). However, the generally good to excellent fits to the literature prion aggregation kinetic data (i.e., specifically to the data which shows sigmoidal behavior) by the F−W two-step model demonstrated herein were achieved without specifically including fragmentation. These two seemingly inconsistent facts (the literature evidence for fragmentation, *op. cit.*, vs the lack of a specific step to account for fragmentation in the F−W two-step model) require thought and subsequent comment.

Three logical hypotheses seem possible here: (i) fragmentation is not really a part of at least the kinetic pathway for prion aggregation as previously believed; we believe, however, that this idea cannot be right in light of the extant evidence for fragmentation (*51*−*55*). (ii) A second thought is that too little is known at present about the true products and their structures of prion aggregation versus time to make a definitive statement about the role of fragmentation in the mechanism of prion aggregation. A related issue here is that fibers are believed to grow from one or both ends only (*56*−*58*). If fibers grow from only their ends, and if B is the growth surface, then one would expect the growth step to be expressed as "A + B → B" instead of "A + B → 2B". However, this stoichiometry per se can be ruled out as it is inconsistent with the observed autocatalytic curves [i.e., with the need for A + B → 2B (the kinetic definition of autocatalysis) as the second step of the F−W kinetic model]. (iii) A third more likely hypothesis in our opinion is that the F−W two-step model may be "hiding" fragmentation somehow. For example, if the number of fiber ends closely parallels the total amount of aggregated protein, which was predicted in one model of Sup35p aggregation (*54*), then B would be approximately proportional to the growth surface, effectively hiding fragmentation in "B". A related issue here is that the way a particular physical method monitors "growth" may be hiding fragmentation within the description of B. Again, the need for additional studies is apparent (*41*).

*Examination of Four Prior Mechanisms for Prion Transmission and Propagation.* Four prior mechanisms have been suggested for the transmission and propagation of prions, as briefly discussed in the introductory section and summarized in Table 1. Attempts have been made in the prion literature to test the validity of these mechanisms (*23, 59*).[7] In our view, all four mechanisms present valid and alternative descriptions of prion aggregation at the molecular level; however, none can be ruled out at present. Attempts to rule out any of these four mechanisms by using kinetic data both (a) have not been done, and (b) will not be possible until these word/picture mechanisms are turned into specific reactions, defining individual, specific rate constants that can then be used to derive differential or integrable rate equations for actual data fitting.[6] Nevertheless, in time, the true picture of prion aggregation at the molecular level may turn out to contain features from all four mechanisms.

*Caveats and Limitations of the F−W Model.* The F−W model appears to fit a broad range of kinetic aggregation data (*31, 42*−*47*), including amyloid-$\beta$, $\alpha$-synuclein, polyglutamine, and now the prion protein aggregation systems. However, and as previously addressed (*31*), the F−W model has limitations:

(i)The F−W two-step model is obviously a highly condensed, oversimplified, *phenomenological kinetic model* of the real, molecular prion aggregation process that probably consists of hundreds if not thousands of steps in most cases.

(ii) The resultant $k_1$ and $k_2$ values are, therefore, averages over all of the true underlying steps. As such, important kinetic and mechanistic information must be hidden in the average A → B and A + B → 2B pseudoelementary steps and their resultant, average $k_1$ and $k_2$ rate constants.

(iii) Another issue is that during the nucleation process, [A] is approximately constant. Therefore, a higher kinetic order in [A], that is $k_1'[A]^n$, is easily hidden kinetically and can appear as an apparent $k_{1(\text{apparent})}[A]$ dependence, where in fact $k_{1(\text{apparent})} = k_1'[A]^{n-1}$ (*60*). A study of any concentration dependence of $k_{1(\text{apparent})}$ can be used to overcome this issue, however.

[7] Attempts have been made in the yeast prion literature to test the validity of these four (molecular) mechanisms by looking at the effect of yeast protein concentration on the observed lag times and aggregation rates of the protein in its prion form. There, for each mechanism, the authors state expected correlations between the observed lag times/aggregation rates and initial protein concentration that are essentially qualitative in nature. The authors often then use these stated expectations quantitatively, as a proposed way to test the likelihood of each mechanism. We will argue that these correlations were derived in a manner that is not strictly proper kinetically, since a kinetically rigorous treatment would require that (i) chemical equations be written, (ii) appropriate rate equations be given, and, where possible, (iii) either numerical integration be used, or integrated rate equations be provided and used.

(iv) Finally, the fact that all sizes of the growing aggregate are hidden behind the general descriptor B, while a great advantage for extracting an average $k_2$, hides important molecular details that will need to be the focus of separate studies. The possible role of fragmentation in the proper description of B versus time is a related issue here, again one requiring future studies.

In light of the limitations described above, we have attempted to be cautious in the interpretations herein and urge others to similarly use caution when interpreting results from the F−W model.

## CONCLUSIONS

In conclusion, the main contributions from this paper can be summarized as follows.

(i) Twenty-seven prion aggregation curves from the literature, measured by seven different physical methods, were successfully fit using the F−W model, allowing for the deconvolution of average nucleation ($k_1$) and growth ($k_2$) kinetic parameters for the first time in all cases.

(ii) The F−W model was able to fit the in vitro aggregation curves of three different types of yeast prions, as well as that of mouse and human prion.

(iii) The aggregation of Sup35p measured by six different physical methods under the same experimental conditions (*23*), fit by the F−W model, provided values of the nucleation and growth rate constants that were equivalent within experimental error. This is an important study (*23*), and the $k_1$ and $k_2$ analysis provided herein yields considerably more confidence than before that true aggregation rates (and now, $k_1$ and $k_2$ rate constants) can be faithfully measured using different methods, at least for this Sup35p system.

(iv) Fits of Sup35p aggregation curves by the F−W model indicate the hypotheses requiring further study that (i) the Glu/Asn rich N-terminal region of the prion domain appears to influence the kinetics of nucleation more than growth and (ii) the oligopeptide repeat-containing C-terminal region of the prion domain appears to affect the kinetics of growth more than nucleation.

(v) Fits of Ure2p aggregation curves by the F−W model indicate the hypothesis that Gln/Asn rich regions in the prion domain of this protein appear to influence the kinetics of nucleation more than growth.

(vi) Examination of four prior mechanisms suggested for prion transmission and propagation reveals that these prior mechanisms, while useful molecular descriptions, have not yet been turned into useful kinetic models that can be used for fitting data and, thereby, distinguishing those postulated (molecular) mechanisms from one another.

(vii) The F−W model provides, therefore, the presently available kinetic model/minimal kinetic mechanism of prion aggregation and its average nucleation ($k_1$) and growth ($k_2$) rate constants.

(viii) Caveats of the F−W model were discussed, particularly the facts that (a) since each pseudoelementary step hides many (sub)steps at the molecular level, the rate constants obtained for nucleation and growth are actually average rate constants and (b) the average nature of B also hides potentially important data about fibril size versus time effects, including the possible contributions of fragmentation effects.

(ix) Hence, the need for future experimental work on the issues of agitation and fragmentation was noted.

(x) Also included in the needed future experiments are more direct experiments on what A and B are in prion aggregation, and B versus time. How do those A and B relate to the molecular descriptions in the previously suggested mechanisms in Table 1? These issues, and the three hypotheses given in the Discussion, should provide fertile ground for future studies.

## ACKNOWLEDGMENT

It is important to specifically acknowledge and thank all the research groups and authors listed in the references and Table 1. Those authors, and not us, provided the primary experimental and other data which were analyzed herein. Without their original efforts, nothing reported herein would have been possible.

## SUPPORTING INFORMATION AVAILABLE

Raw, digitized data (i.e., not normalized to an initial minimum of zero) corresponding to Figures 2−7, 9, and 10 of the main text along with their fits to the F−W model and ensuing discussion on the observed effects of agitation on the aggregation curve of Sup35p. This material is available free of charge via the Internet at http://pubs.acs.org.

## REFERENCES

1. Prusiner, S. B., Scott, M. R., DeArmond, S. J., and Cohen, F. E. (1998) Prion protein biology. *Cell 93*, 337–348.
2. Prusiner, S. B. (1982) Novel proteinaceous infectious particles cause scrapie. *Science 216*, 136–144.
3. Somerville, R. A., Bendheim, P. E., and Bolton, D. C. (1991) The transmissible agent causing scrapie must contain more than protein. *Rev. Med. Virol. 1*, 131–139.
4. Weissmann, C. (1991) A 'unified theory' of prion propagation. *Nature 352*, 679–683.
5. Lieberman, M., Marks, A. D., and Smith, C. (2007) *Marks' Essentials of Medical Biochemistry. A Clinical Approach*, Lippincott Williams & Wilkins, Baltimore.
6. Wickner, R. B., Edskes, H. K., Shewmaker, F., and Nakayashiki, T. (2007) Prions of fungi: Inherited structures and biological roles. *Nat. Rev. Microbiol. 5*, 611–618.
7. Ross, E. D., Minton, A., and Wickner, R. B. (2005) Prion domains: Sequences, structures and interactions. *Nat. Cell Biol. 7*, 1039–1044.
8. Wickner, R. B., Edskes, H. K., Roberts, B. T., Baxa, U., Pierce, M. M., Ross, E. D., and Brachmann, A. (2004) Prions: Proteins as genes and infectious entities. *Genes Dev. 18*, 470–485.
9. Wickner, R. B. (1994) [URE3] as an altered URE2 protein: Evidence for a prion analog in *Saccharomyces cerevisiae*. *Science 264*, 566–569.
10. Chernoff, Y. O., Derkach, I. L., and Ingevechtomov, S. G. (1993) Multicopy Sup35 gene induces *de novo* appearance of *PSI*-like factors in the yeast *Saccharomyces cerevisiae*. *Curr. Genet. 24*, 268–270.
11. Derkatch, I. L., Bradley, M. E., Hong, J. Y., and Liebman, S. W. (2001) Prions affect the appearance of other prions: The story of [PIN(+)]. *Cell 106*, 171–182.
12. Patel, B. K., and Liebman, S. W. (2007) "Prion-proof" for [*PIN*+]: Infection with *in vitro*-made amyloid aggregates of Rnq1p-(132−405) induces [*PIN*+]. *J. Mol. Biol. 365*, 773–782.
13. Brachmann, A., Baxa, U., and Wickner, R. B. (2005) Prion generation *in vitro*: Amyloid of Ure2p is infectious. *EMBO J. 24*, 3082–3092.
14. Tanaka, M., Chien, P., Naber, N., Cooke, R., and Weissman, J. S. (2004) Conformational variations in an infectious protein determine prion strains differences. *Nature 428*, 323–328.
15. King, C. Y., and Diaz-Avalos, R. (2004) Protein-only transmission of three yeast prion strains. *Nature 428*, 319–323.

16. Atwood, C. S., Obrenovich, M. E., Liu, T. B., Chan, H., Perry, G., Smith, M. A., and Martins, R. N. (2003) Amyloid-$\beta$: A chameleon walking in two worlds: A review of the trophic and toxic properties of amyloid-$\beta$. *Brain Res. Rev. 43*, 1–16.
17. Walsh, D. M., and Selkoe, D. J. (2007) A$\alpha$ oligomers: A decade of discovery. *J. Neurochem. 101*, 1172–1184.
18. Ferreira, S. T., Vieira, M. N. N., and Felice, F. G. D. (2007) Soluble protein oligomers as emerging toxins in Alzheimer's and other amyloid diseases. *IUBMB Life 59*, 332–345.
19. Fink, A. L. (2006) The aggregation and fibrillation of $\alpha$-synuclein. *Acc. Chem. Res. 39*, 628–634.
20. Walsh, D. M., Lomakin, A., Benedek, G. B., Condron, M. M., and Teplow, D. B. (1997) Amyloid $\beta$-protein fibrillogenesis: Detection of a protofibrillar intermediate. *J. Biol. Chem. 272*, 22364–22372.
21. Harper, J. D., Wong, S. S., Lieber, C. M., and Lansbury, P. T., Jr. (1997) Observation of metastable A$\beta$ amyloid protofibrils by atomic force microscopy. *Chem. Biol. 4*, 119–125.
22. Gosal, W. S., Morten, I. J., Hewitt, E. W., Smith, D. A., Thomson, N. H., and Radford, S. E. (2005) Competing pathways determine fibril morphology in the self-assembly of $\beta_2$-microglobulin into amyloid. *J. Mol. Biol. 351*, 850–864.
23. Serio, T. R., Cashikar, A. G., Kowal, A. S., Sawicki, G. J., Moslehi, J. J., Serpell, L., Arnsdorf, M. F., and Lindquist, S. L. (2000) Nucleated conformational conversion and the replication of conformational information by a prion determinant. *Science 289*, 1317–1321.
24. Eigen, M. (1996) Prionics or the kinetic basis of prion diseases. *Biophys. Chem. 63*, A1–A18.
25. Prusiner, S. B. (1991) Molecular biology of prion diseases. *Science 252*, 1515–1522.
26. Cohen, F. E., Pan, K.-E., Huang, Z., Baldwin, M., Fletterick, R. J., and Prusiner, S. B. (1994) Structural clues to prion replication. *Science 264*, 530–531.
27. Come, J. H., Fraser, P. E., and Lansbury, P. T. (1993) A kinetic model for amyloid formation in the prion diseases. Importance of seeding. *Proc. Natl. Acad. Sci. U.S.A. 90*, 5959–5963.
28. Jarrett, J. T., and Lansbury, P. T. (1993) Seeding "one-dimensional crystallization" of amyloid: A pathogenic mechanism in Alzheimer's disease and scrapie? *Cell 73*, 1055–1058.
29. Griffith, J. S. (1967) Self-replication and scrapie. *Nature 215*, 1043–1044.
30. Morris, A. M., Watzky, M. A., and Finke, R. G. (2008) Protein aggregation kinetics, mechanism, and curve-fitting: A critical review of the literature. *Biochim. Biophys. Acta* (submitted for publication).
31. Morris, A. M., Watzky, M. A., Agar, J. N., and Finke, R. G. (2008) Fitting neurological protein aggregation kinetic data via a 2-step, minimal/"Ockham's razor" model: The Finke-Watzky mechanism of nucleation followed by autocatalytic surface growth. *Biochemistry 47*, 2413–2427.
32. Santoso, A., Chien, P., Osherovich, L. Z., and Weissman, J. S. (2000) Molecular basis of a yeast prion species barrier. *Cell 100*, 277–288.
33. DePace, A. H., Santoso, A., Hillner, P., and Weissman, J. S. (1998) A critical role for amino-terminal glutamine/asparagines repeats in the formation and propagation of a yeast prion. *Cell 93*, 1241–1252.
34. Liu, J.-J., and Lindquist, S. L. (1999) Oligopeptide-repeat expansions modulate 'protein-only' inheritance in yeast. *Nature 400*, 573–576.
35. Osherovich, L. Z., Cox, B. S., Tuite, M. F., and Weissman, J. S. (2004) Dissection and design of yeast prions. *PLoS Biol. 2*, 442–451.
36. Jiang, Y., Li, H., Zhu, L., Zhou, J.-M., and Perrett, S. (2004) Amyloid nucleation and hierarchical assembly of Ure2p fibrils. *J. Biol. Chem. 279*, 3361–3369.
37. Ross, E. D., Edskes, H. K., Terry, M. J., and Wickner, R. B. (2005) Primary sequence independence for prion formation. *Proc. Natl. Acad. Sci. U.S.A. 102*, 12825–12830.
38. Zhu, L., Zhang, X. J., Wang, L. Y., Zhou, J. M., and Perrett, S. (2003) Relationship between stability of folding intermediates and amyloid formation for the yeast prion Ure2p: A quantitative analysis of the effects of pH and buffer system. *J. Mol. Biol. 328*, 235–254.
39. Baskakov, I. V., Legname, G., Prusiner, S. B., and Cohen, F. E. (2001) Folding of prion protein to its native $\alpha$-helical conformation is under kinetic control. *J. Biol. Chem. 276*, 19687–19690.
40. Baskakov, I. V., and Bocharova, O. V. (2005) In vitro conversion of mammalian prion protein into amyloid fibrils displays unusual features. *Biochemistry 44*, 2339–2348.
41. Watzky, M. A., Morris, A. M., Ross, E. D., and Finke, R. G., studies in progress.
42. Watzky, M. A., and Finke, R. G. (1997) Transition metal nanocluster formation kinetic and mechanistic studies. A new mechanism when hydrogen is the reductant: Slow, continuous nucleation and fast autocatalytic surface growth. *J. Am. Chem. Soc. 119*, 10382–10400.
43. Aiken, J. D., III, and Finke, R. G. (1998) Nanocluster formation synthetic, kinetic, and mechanistic studies. The detection of, and then methods to avoid, hydrogen mass-transfer limitations in the synthesis of polyoxoanion- and tetrabutylammonium-stabilized, near-monodisperse 40 $\pm$ 6 Å Rh(0) nanoclusters. *J. Am. Chem. Soc. 120*, 9545–9554.
44. Widegren, J. A., Aiken, J. D., III, Özkar, S., and Finke, R. G. (2001) Additional investigations of a new kinetic method to follow transition-metal nanocluster formation, including the discovery of heterolytic hydrogen activation in nanocluster nucleation reactions. *Chem. Mater. 13*, 312–324.
45. Hornstein, B. J., and Finke, R. G. (2004) Transition-metal nanocluster kinetic and mechanistic studies emphasizing nanocluster agglomeration: Demonstration of a kinetic method that allows monitoring of all three phases of nanocluster formation and aging. *Chem. Mater. 16*, 139–150, 3972 (Erratum).
46. Besson, C., Finney, E. E., and Finke, R. G. (2005) A mechanism for transition-metal nanoparticle self-assembly. *J. Am. Chem. Soc. 127*, 8179–8184.
47. Besson, C., Finney, E. E., and Finke, R. G. (2005) Nanocluster nucleation, growth, and then agglomeration kinetic and mechanistic studies: A more general, four-step mechanism involving double autocatalysis. *Chem. Mater. 17*, 4925–4938.
48. Field, R. J., and Noyes, R. M. (1977) Oscillations in chemical systems. 18. Mechanisms of chemical oscillators: Conceptual bases. *Acc. Chem. Res. 10*, 214–221.
49. Ross, E. D., Baxa, U., and Wickner, R. B. (2004) Scrambled prion domains form prions and amyloid. *Mol. Cell. Biol. 24*, 7206–7213.
50. Chien, P., DePace, A. H., Collins, S. R., and Weissman, J. S. (2003) Generation of prion transmission barriers by mutational control of amyloid conformations. *Nature 424*, 948–951.
51. Paushkin, S. V., Kushnirov, V. V., Smirnov, V. N., and Ter-Avanesyan, M. D. (1996) Propagation of the yeast prion-like [psi+] determinant is mediated by oligomerization of the SUP35-encoded polypeptide chain release factor. *EMBO J. 15*, 3127–3134.
52. Tanaka, M., Collins, S. R., Toyama, B. H., and Weissman, J. S. (2006) The physical basis of how prion conformations determine strain phenotypes. *Nature 442*, 585–589.
53. Ness, F., Ferreira, P., Cox, B. S., and Tuite, M. F. (2002) Guanidine hydrochloride inhibits the generation of prion "seeds" but not prion protein aggregation in yeast. *Mol. Cell. Biol. 22*, 5593–5605.
54. Collins, S. R., Douglass, A., Vale, R. D., and Weissman, J. S. (2004) Mechanism of prion propagation: Amyloid growth occurs by monomer addition. *PLoS Biol. 2*, 1582–1590.
55. Wegrzyn, R. D., Bapat, K., Newnam, G. P., Zink, A. D., and Chernoff, Y. O. (2001) Mechanism of prion loss after Hsp104 inactivation in yeast. *Mol. Cell. Biol. 21*, 4656–4669.
56. Scheibel, T., Kowal, A. S., Bloom, J. D., and Lindquist, S. L. (2001) Bidirectional amyloid fiber growth for a yeast prion determinant. *Curr. Biol. 11*, 366–369.
57. Inoue, Y., Kishimoto, A., Hirao, J., Yoshida, M., and Taguchi, H. (2001) Strong growth polarity of yeast prion fiber revealed by single fiber imaging. *J. Biol. Chem. 276*, 35227–35230.
58. DePace, A. H., and Weissman, J. S. (2002) Origins and kinetic consequences of diversity in Sup35 yeast prion fibers. *Nat. Struct. Biol. 9*, 389–396.
59. Kelly, J. W. (2000) Mechanisms of amyloidogenesis. *Nat. Struct. Biol. 7*, 824–826.
60. Watzky, M. A., Ott, L. S., Finney, E. E., and Finke, R. G., studies in progress.

BI800726M